

Effect of sulfur on the polymorphism and reactivity of dicalcium silicate of Portland clinker

(Efeito do enxofre no polimorfismo e reatividade do silicato dicálcico do clínquer Portland)

F. R. D. Andrade¹, S. D. Gomes², M. Pecchio³, Y. Kihara^{1,3}, F. M. S. Carvalho¹, J. R. Matos⁴

¹Departamento de Mineralogia e Geotectônica, Instituto de Geociências, Universidade de S. Paulo, Rua do Lago 562 S. Paulo, SP 05508-900

²Rua Sta. Maria Itabira 100/01, Belo Horizonte, MG 30310-600

³Associação Brasileira de Cimento Portland, Av. Torres de Oliveira 76, S. Paulo, SP 05347-902

⁴Departamento de Química Fundamental, Instituto de Química, Universidade de S. Paulo, Av. Prof. Lineu Prestes 748, S. Paulo, SP 05508-000
dias@usp.br

Abstract

The present study regards the effect of sulfur in dicalcium silicate (Ca_2SiO_4), a major crystalline phase (20 to 40 wt.%) of the ordinary Portland cement clinker. Dicalcium silicate is also known as C_2S ($2\text{CaO}\cdot\text{SiO}_2$) or belite. The synthesis of the C_2S samples was made with high purity reactants with addition of sulfur as $\text{CaSO}_4\cdot 2\text{H}_2\text{O}$, mixed according to the stoichiometric proportion $2\text{Ca}:(1-x)\text{Si}:x\text{S}$, in which x corresponds to the cationic proportion of sulfur, with values ranging from 0 to 20%. Added amounts of SO_3 in the samples were 0.23, 1.39, 2.77, 4.60 and 9.71 wt.%. Chemical composition of the samples was determined by X-ray fluorescence before and after sintering. Large-scale sulfur loss by volatilization leads to an excess in calcium and consequently to formation of increasing amounts of tricalcium silicate with increasing sulfur content in the starting mixture. Mineralogical composition of the samples and cell parameters of C_2S polymorphs were determined by X-ray diffraction and Rietveld refinements. Structural analysis of diffraction data indicates that the presence of sulfur stabilizes the intermediate temperature polymorph β C_2S , with increasing unit cell volume. The reactivity with water (heat of hydration) of the samples was measured by differential scanning calorimetry, which was strongly influenced by the highly reactive tricalcium silicate.

Keywords: dicalcium silicate, Portland clinker, sulfur, polymorphism, XRD-Rietveld, DSC calorimetry.

Resumo

Este estudo trata do efeito do enxofre no silicato de dicálcio (Ca_2SiO_4), uma fase cristalina majoritária (20 a 40 peso%) do clínquer do cimento Portland comum. O silicato de dicálcio é também conhecido como C_2S ($2\text{CaO}\cdot\text{SiO}_2$) ou belita. A síntese de amostras de C_2S foi feita a partir de reagentes de alta pureza com adição de enxofre como $\text{CaSO}_4\cdot 2\text{H}_2\text{O}$, misturados na proporção estequiométrica $2\text{Ca}:(1-x)\text{Si}:x\text{S}$, na qual x corresponde à proporção catiônica de enxofre, com valores de 0 a 20%. Os teores adicionados de SO_3 nas amostras foram 0,23, 1,39, 2,77, 4,60 e 9,71 peso%. A composição química das amostras foi determinada por meio de fluorescência de raios X antes e após sinterização. A perda por volatilização em alta escala de enxofre levou a um excesso de cálcio e conseqüentemente à formação crescente de silicato de tricálcio com aumento crescente de enxofre na mistura inicial. A composição mineralógica das amostras e os parâmetros de rede dos polimorfos de C_2S foram determinados por difração de raios X e refinamento de Rietveld. A análise estrutural dos resultados de difração indica que a presença de enxofre estabiliza a forma de temperatura intermediária β C_2S , com aumento crescente do volume da célula unitária. A reatividade com água (calor de hidratação) das amostras foi medido por calorimetria diferencial de varredura, que foi fortemente influenciado pela alta reatividade do silicato de tricálcio.

Palavras-chave: silicato de dicálcio, clínquer de Portland, enxofre, polimorfismo, difração de raios X, análise de Rietveld, calorimetria diferencial de varredura.

INTRODUCTION

The role of sulfur in the Portland cement industry has been extensively investigated in the last decades, because of its major effects in all stages of the cement life-cycle, from clinker mineralogy, through cement performance up to

concrete degradation. The sources of sulfur in the context of cement production are raw materials and fuels, particularly pet coke, in which the sulfur content may reach up to 6wt.% [1]. Sulfur may be present in the raw materials as sulfides, mainly the iron sulfide pyrite, which is likely to increase sulfur emissions, since sulfur volatility largely depends on

its oxidation state, and sulfides are considered to be more volatile than sulfates [2].

Among the main crystalline phases of clinker, dicalcium silicate (Ca_2SiO_4) has the higher capacity of sulfur incorporation [3]. In the presence of alkalis, sulfur preferentially forms alkali sulfates such as arcanite (K_2SO_4), ca-langbeinite ($\text{K}_2\text{Ca}_2(\text{SO}_4)_3$) and aphtitalite ($\text{K}_3\text{Na}(\text{SO}_4)_2$) [4]. In the presence of sulfur, the relative proportion of dicalcium silicate in clinker increases, with respective decrease in tricalcium silicate abundance, which tends to form larger crystals [5]. These changes in texture and phase relations of Portland clinker lead to lowering in grindability and delaying in setting time.

Sulfur is also added at the final stage of Portland cement production, when the clinker pellets are grinded together with ca. 5 wt.% of gypsum ($\text{CaSO}_4 \cdot 2\text{H}_2\text{O}$), which retard the hydration reactions that eventually lead to cement setting (hardening). Sulfur may also be related to concrete degradation, in a process known as sulfate attack. An extensive review on the subject is given [6]. Although the topic is still under debate, sulfate attack is likely to be related to external sources of sulfur, and not by the relatively small amount of the element present in the cement [3].

In the following text, the abbreviated forms of clinker phases are used: C = CaO, S = SiO_2 , A = Al_2O_3 and F = Fe_2O_3 . Dicalcium silicate ($2\text{CaO} \cdot \text{SiO}_2$) will be referred from now on as C_2S , and tricalcium silicate ($3\text{CaO} \cdot \text{SiO}_2$) as C_3S . Hydrated calcium silicates are referred to as CSH ($\text{CaO} \cdot \text{SiO}_2 \cdot n\text{H}_2\text{O}$). Further effects of sulfur on clinker mineralogy comprise polymorphism of dicalcium silicate and, therefore, its reactivity with water [7]. C_2S has five polymorphs: γ , β , α_L , α_H and α , in order of stability at increasing temperature [8-10]. Polymorphic transformations of C_2S are of interest in cement industry, because the polymorphs of higher temperature, which are more reactive with water, may be stabilized by the incorporation of minor elements [11, 12] or thermal treatment [13]. Increasing reactivity of C_2S is a relevant issue in large-scale production of C_2S -rich cements [14, 15], which is a low-energy and low-emission option to ordinary portland cement, that is mainly composed by C_3S , the most reactive calcium silicate in clinker. The polymorph β C_2S predominates in ordinary portland cement and has a rather slow hydration kinetic, leading to lower mechanical strength at early ages [7].

This paper presents experimental results on the effects of sulfur in polymorphic transformation and hydraulic reactivity of C_2S in the presence of sulfur.

MATERIALS AND METHODS

Six samples were produced by sintering mixtures of the following high purity reactants: CaCO_3 99.0% Merck; $\text{CaSO}_4 \cdot 2\text{H}_2\text{O}$ 99.0% Merck; silica gel $\text{SiO}_2 \cdot x\text{H}_2\text{O}$ 99.99% Vetec, with 9.1 wt.% loss on ignition at 1000 °C. Stoichiometry of the starting mixtures was set according to $2\text{Ca} \cdot (1-x)\text{Si} : x\text{S}$, where x varied between 0 and 2 (Table I), considering the substitution of S for Si in the tetrahedral structural site of

the silicate (see Discussion). Reactants were homogenized in tungsten carbide vibratory mill and sintered in platinum crucibles under oxidant conditions in a chamber furnace. In the first step, samples were calcined at 900 °C, ground for 20 s, and pressed in a hydraulic press under 39 MPa (20.000 kg on a 40 mm diameter disc). In the second step, samples were sintered at 1450 °C for 6 h, with two intermediate milling and pressing steps, according to the procedures described [12]. After sintering, samples were immediately cooled with air, in order to preserve high temperature crystalline phases. After cooling to room temperature, samples were ground in a tungsten carbide vibratory disk mill for 20 s and split in aliquots for further analysis.

Table I - Predicted stoichiometric proportion of the raw mixtures.

[Tabela I - Proporção estequiométrica prevista para as misturas cruas.]

sample	structural formula
BS 0	$\text{Ca}_2\text{Si}_1\text{S}_0\text{O}_4$
BS 0.5	$\text{Ca}_2\text{Si}_{0.995}\text{S}_{0.005}\text{O}_4$
BS 3	$\text{Ca}_2\text{Si}_{0.97}\text{S}_{0.03}\text{O}_4$
BS 6	$\text{Ca}_2\text{Si}_{0.94}\text{S}_{0.06}\text{O}_4$
BS 10	$\text{Ca}_2\text{Si}_{0.90}\text{S}_{0.10}\text{O}_4$
BS 20	$\text{Ca}_2\text{Si}_{0.80}\text{S}_{0.20}\text{O}_4$

X-ray powder diffraction (XRD) was carried out in a Rigaku RINT2000 equipment with $\text{CuK}\alpha$ radiation, 40 kV, 30 mA, step scanning mode (0.01°/step, 10 s/step) from 18 to 90° 2 θ . Samples were front loaded in flat sample holders. Instrumental contribution to peak broadening was assessed with a cerium oxide (CeO_2) standard [16]. Rietveld refinements were carried out in GSAS [17] with the graphic user interface EXPGUI [18]. The crystallographic informations files (CIF) for C_2S polymorphs were taken from [9] and for triclinic C_3S from [19]. Rietveld refinement strategy was based on [20, 21] and Paiva-Santos (personal communication), comprising background fitting with the shifted Chebyshev function (10 terms), cell parameters, scale factors for individual phases, peak displacement (shift), surface roughness correction, isotropic atomic displacement parameter (Uiso), pseudo-Voigt function of peak profile (GSAS #4) and spherical harmonic preferential orientation for all phases.

Differential scanning calorimetry (DSC) was analyzed in a Shimadzu DSC50 calorimeter with aluminum crucibles, with constant rate of temperature increase (10 °C/min) from room temperature to 500 °C, in a dynamic atmosphere of nitrogen flow (50 mL/min). Samples were ground down to > 0.045 mm and their grain-size was controlled by sieving. An amount of 5 g of each sample was mixed in distilled water in a water/sample mass ratio of 0.4 and stored at 40 °C for 80 h to achieve full hydration and formation of portlandite ($\text{Ca}(\text{OH})_2$) and hydrated calcium silicates (CSH).

After hydration, samples were milled and dried at 200 °C for 24 h. An 8 mg aliquot from each sample was used for DSC analysis. This reverse calorimetric analysis measures the amount of heat absorbed by the sample to transform the hydrated phases back in the anhydrous Ca-silicates, *i.e.*, the more reactive samples form more CSH and portlandite and, therefore, absorb more heat in their dehydration.

Chemical analyses were made in a Rigaku - RIX 2000 X-ray fluorescence (XRF) equipment, with tube conditions of 50 kV and 50 mA, in samples prepared as fused glass discs. Calibration was made with seven standard cements from the National Institute of Standards and Technology (NIST) and two from the Instituto de Pesquisas Tecnológicas, S. Paulo, Brazil (IPT). Sulfur loss was controlled by chemical analysis of raw mixtures and sintered samples.

RESULTS AND DISCUSSION

Chemical composition of the samples before and after sintering is presented in Table II. Actual chemical composition of raw mixtures determined by XRF is very close to the predicted stoichiometric proportions established in Table I. It indicates that there was no sulfur loss until 1000 °C, the temperature in which the glass discs were prepared for XRF analysis.

After sintering at 1450 °C, the expected stoichiometry of the samples (Table I) was not achieved, due to extreme sulfur loss by volatilization (between 80 and 100 wt.%), leading to a relative excess in CaO in respect to the (SO₃+SiO₂) and to C₃S formation.

Progressive changes in composition may be seen by comparing diffractograms of all samples (Fig. 1). The main diffraction peak of the three phases (γ C₂S, β C₂S, C₃S tcl) overlap between 31.9 and 32.0° 2 θ (CuK α) and, therefore, the mineralogical changes are present in the secondary peaks

indicated in the lower part of the diffractogram.

A good adjustment was achieved between observed diffractograms and calculated models, as indicated by the difference line in Rietveld plots (Fig. 2) and by the low values of statistical residues of the Rietveld refinements (Table III). Modal composition obtained by XRD-Rietveld is presented in Fig. 3 and Table III. The increase in the amount of sulfur in the raw mixture leads to a decrease of γ C₂S and to a respective increase in the β C₂S. Stabilization of β C₂S by sulfur has been previously described [7]. The stable polymorph at lowest temperature, γ C₂S, is undesired in Portland clinker, because of its lower reactivity with water. Additionally, the polymorphic transition from β to γ C₂S leads to an increase in the molar volume of the silicate, which may cause an effect known as dusting, a process in which the clinker turns spontaneously into powder while cooling [22].

Sulfur loss is probably related to the sequence of thermal decomposition of the reactants with increasing temperature. Thermal decomposition of CaCO₃ takes place in a wide range of temperature, from 660 to 900 °C, and is strongly controlled by the partial pressure of CO₂ [23-25]. Calcium sulfate dihydrate (CaSO₄.2H₂O) undergoes stepwise thermal decomposition, with progressive loss of water from 60 to 450 °C [26]. Increasing temperature leads to formation of hemihydrate and other intermediate hydrated compounds before total dehydration. Anhydrous calcium sulfate remains stable until 1380 °C, where melting occurs [27]. In the present study, high purity silica gel was used, which is a non-crystalline, reactive form of silica. Therefore, calcium oxide possibly did combine with silica before the sulfate was available by decomposition of anhydrous calcium sulfate at much higher temperature. This unforeseen problem in the experimental project probably explains the difference of our results with those of [2], who concluded that SO₃ has low

Table II - Chemical composition of the samples: B = before sintering (raw mixture); A = after sintering. In the upper part of the table, data are presented as wt.%, together with the sulfur loss (wt.%) after sintering. In the lower part, data are presented as molar proportion normalized to three moles (2CaO.SiO₂).

[Tabela II - Composição química das amostras: B = pré-sinterização (mistura crua); A = pós-sinterização. Na parte superior da tabela, os dados são apresentados em % em peso, juntamente com a perda de enxofre (% em peso) após a sinterização. Na parte inferior da tabela os dados são apresentados em proporção molar normalizada para três moles (2CaO.SiO₂).]

	BS 0		BS 0.5		BS 3		BS 6		BS 10		BS 20	
wt %	B	A	B	A	B	A	B	A	B	A	B	A
CaO	65.1	65.3	65.1	65.1	64.9	65.9	64.7	66.6	64.4	67.7	61.2	69.5
SiO ₂	34.9	34.4	34.7	33.9	33.7	33.7	32.6	32.8	31.0	31.5	29.1	29.6
SO ₃	0	0	0.23	0	1.39	0.07	2.77	0.50	4.6	0.86	9.71	0.89
sulfur loss wt.%				100		95.0		82.0		81.3		90.8
molar proportion												
CaO	2.000	2.011	2.000	2.019	2.000	2.030	2.000	2.050	2.001	2.079	1.928	2.133
SiO ₂	1.000	0.989	0.995	0.981	0.970	0.961	0.940	0.941	0.899	0.903	0.857	0.848
SO ₃	0.000	0.000	0.005	0.000	0.030	0.002	0.060	0.011	0.100	0.018	0.215	0.019

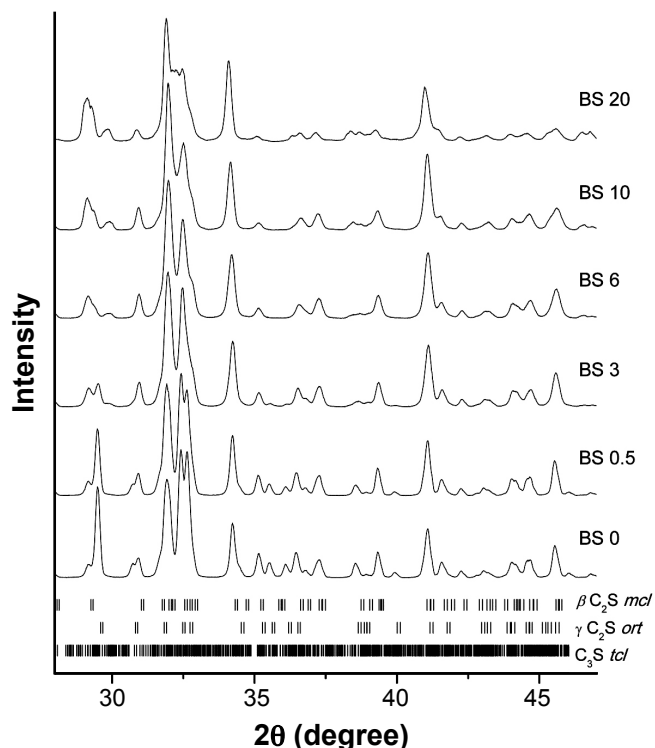


Figure 1: Selected angular (2-theta) range of X-ray diffraction patterns of the sintered samples, with indication of diffraction peak positions for the phases.

[Figura 1: Faixa angular (2-teta) selecionada dos difratogramas de raios X das amostras sinterizadas, com indicação da posição dos picos de difração das fases.]

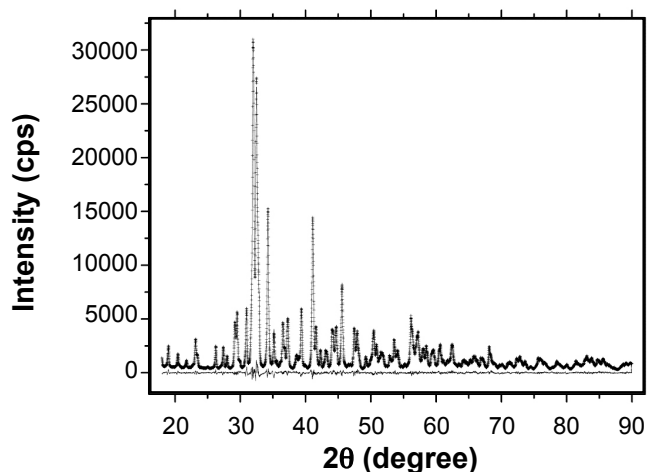


Figure 2: Rietveld plot of a selected sample (BS 3); observed (crosses), calculated (continuous line) and difference curve (bottom line).

[Figura 2: Diagrama de Rietveld de amostra selecionada (BS 3); observado (cruzes), calculado (linha contínua) e curva de diferença (linha inferior).]

volatility while S has high volatility. As already mentioned, XRF chemical data (Table II) indicate that sulfur loss did not take place up to 1000 °C, the temperature in which fused glass discs were prepared.

Major changes in cell parameters with increasing sulfur

Table III - Mineralogical composition (wt.%) determined by XRD-Rietveld, and respective statistical parameters of Rietveld refinements (χ^2 , Rwp); for details see [20]. Numbers in parentheses are the standard uncertainties calculated by the software (GSAS).

[Tabela III - Composição mineralógica (% em peso) determinada por difração de raios X (Rietveld) e respectivos parâmetros estatísticos dos refinamentos pelo método de Rietveld (χ^2 , Rwp); para detalhes consulte [20]. Os números entre parênteses representam a incerteza padrão calculada pelo programa (GSAS).]

sample	$\gamma\text{C}_2\text{S}$	$\beta\text{C}_2\text{S}$	C_3S (triclinic)	χ^2	Rwp
BS0	43.5(5)	56.5(5)	-	4.684	0.0541
BS0.5	33.6(4)	66.4(3)	-	5.204	0.0573
BS3	9.5(5)	78.4(3)	12.1(7)	3.841	0.0493
BS6	-	78.1(3)	21.8(7)	4.179	0.0520
BS10	-	60.0(9)	39.0(1)	5.079	0.0576
BS20	-	36.5(5)	63.4(6)	9.181	0.0768

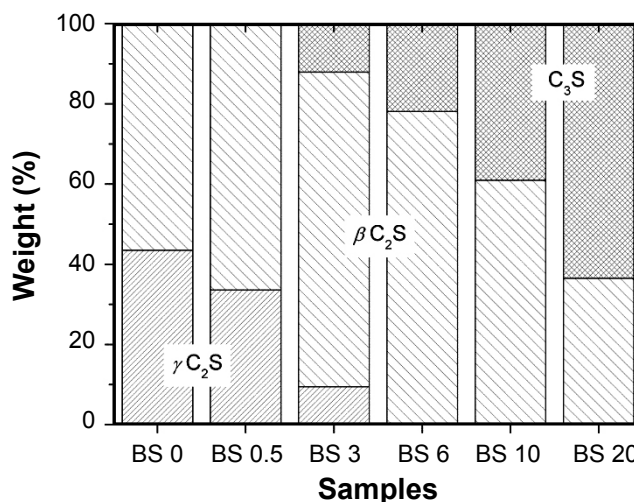


Figure 3: Mineralogical composition (wt.%) of the samples after sintering, determined by XRD-Rietveld.

[Figura 3: Composição mineralógica (% em peso) das amostras após a sinterização, determinada por difração de raios X - Rietveld.]

content were observed in $\beta\text{C}_2\text{S}$ (Fig. 4), in comparison with pure, stoichiometric C_2S [9]. The continuous change in cell parameters with incorporation of sulfur (Table IV) is indicative of assimilation of sulfur as solute in the structure of $\beta\text{C}_2\text{S}$, according to the Vegard's law [28]. Sulfur is likely to occupy the tetrahedral site in substitution for silicon, as both cations have small ionic radius ($\text{Si}^{4+} = 0.26 \text{ \AA}$; $\text{S}^{6+} = 0.12 \text{ \AA}$; after [29]). Variation of cell parameters of $\gamma\text{C}_2\text{S}$ (Table V) is one order of magnitude smaller than those of $\beta\text{C}_2\text{S}$, indicating that sulfur may be present in lower amounts in $\gamma\text{C}_2\text{S}$. Triclinic C_3S in samples BS3 to BS20 does not display relevant or systematic changes in cell parameters in

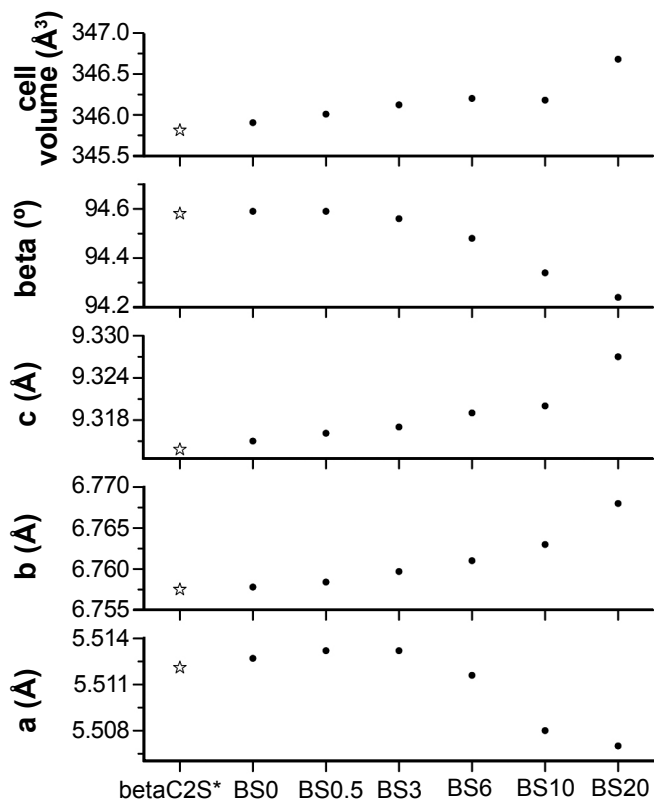


Figure 4: Cell parameters of β C_2S ; beta C2S* refers to the cell parameters of the pure phase [9].

[Figura 4: Parâmetros de cela de β C_2S ; beta C2S* corresponde aos parâmetros de cela da fase pura [9].]

respect with sulfur contents of the samples (Table VI).

Results of differential scanning calorimetry are presented in Table VII. All samples underwent two endothermic events, around 150 °C and 425 °C. The first event refers to loss of adsorbed water from the sample surface and the second reflects dehydration of portlandite and CSH. The amount of heat measured at 425 °C is proportional to the amount of portlandite and CSH in the sample. The heat of hydration of the samples increases steadily with sulfur content. However, this effect is not directly related to the polymorphic transformations of C_2S , but rather to the presence of increasing amounts of C_3S in the samples with sulfur in the raw-mixture. This caused a strong interference in calorimetric measurements, as C_3S has much higher hydration heat (264 J/g; [30]) than β C_2S (17 J/g; [12]) and γ C_2S (8 J/g; [12]), the latter being almost inert. A comparison was made between the observed hydration heat of the samples with the heat of hydration of the pure phases, weighted according to their wt.% in the samples (Table III). An overall good agreement was obtained between observed and calculated hydration heat. A slight increase in hydration heat was observed in the samples BS 0.5, BS 3 and BS 6, which may be related to distortion of β C_2S lattice by sulfur incorporation. In sample B10, there is a disagreement between the measured (82.36 J/g) and the predicted heat (113.16 J/g) of hydration. This is probably due to a propagation of errors, considering the uncertainties in the mineralogical composition (see statistical parameters of the Rietveld refinement in Table III) and the large differences in

Table IV - Cell parameters obtained for β C_2S . The values in the first column (β C_2S^*) correspond to the cell parameters of the pure phase [9]. Numbers in parentheses are the standard uncertainties calculated by the software (GSAS).

[Tabela IV - Parâmetros de cela obtidos para β C_2S . Os valores da primeira coluna (β C_2S^*) correspondem aos parâmetros de cela da fase pura [9]. Os números entre parênteses apresentam a incerteza padrão calculada pelo programa (GSAS).]

	β - C_2S^*	BS 0	BS 0.5	BS 3	BS 6	BS 10	BS 20
a (Å)	5.5121(1)	5.5127(5)	5.5132(5)	5.5132(5)	5.5116(6)	5.508(1)	5.507(2)
b (Å)	6.7575(1)	6.7578(5)	6.7584(5)	6.7597(6)	6.7610(7)	6.763(1)	6.768(2)
c (Å)	9.3138(1)	9.3150(7)	9.3161(7)	9.317(1)	9.319(1)	9.320(2)	9.327(5)
β (°)	94.581(1)	94.59(1)	94.59(1)	94.56(1)	94.48(1)	94.34(2)	94.24(4)
volume (Å ³)	345.812	345.906	346.009	346.150	346.202	346.180	346.679

Table V - Cell parameters obtained for γ C_2S . The values in the first column (γ C_2S^*) correspond to the cell parameters of pure phase, according to [9]. Numbers in parentheses are the standard uncertainties calculated by the software (GSAS).

[Tabela V - Parâmetros de cela obtidos para γ C_2S . Os valores da primeira coluna (γ C_2S^*) correspondem aos parâmetros de cela da fase pura, segundo [9]. Os números entre parênteses apresentam a incerteza padrão calculada pelo programa (GSAS).]

	γ - C_2S^*	BS 0	BS 0.5	BS 3
a (Å)	5.0821(1)	5.0834(4)	5.0836(5)	5.084(1)
b (Å)	11.2237(1)	11.228(1)	11.230(1)	11.233(4)
c (Å)	6.7638(1)	6.7657(7)	6.7665(8)	6.768(3)
volume (Å ³)	385.807	386.162	386.292	386.511

Table VI - Cell parameters obtained for C_3S (triclinic). The values in the first column (C_3S triclinic*) correspond to the cell parameters of pure phase, according to [19]. Numbers in parentheses are the standard uncertainties calculated by the software (GSAS).

[Tabela VI - Parâmetros de cela obtidos para C_3S (triclinico). Os valores da primeira coluna (C_3S triclinic*) correspondem aos parâmetros de cela da fase pura, segundo [19]. Os números entre parênteses representam a incerteza padrão calculada pelo programa (GSAS).]

	C_3S triclinic*	BS 3	BS 6	BS 10	BS 20
a (Å)	11.67	11.6432(6)	11.6460(5)	11.6433(3)	11.6449(2)
b (Å)	14.24	14.2256(6)	14.2208(5)	14.2204(3)	14.2249(2)
c (Å)	13.72	13.7020(9)	13.7020(7)	13.6983(4)	13.7032(3)
α (°)	105.5	105.309(4)	105.272(4)	105.304(2)	105.297(2)
β (°)	94.33	94.619(5)	94.600(4)	94.566(2)	94.559(2)
γ (°)	90	89.778(5)	89.850(6)	89.863(3)	89.864(2)
volume (Å ³)	2190.3	2181.5	2181.7	2180.3	2182.2

Table VII - Endothermic events of dehydration measured by DSC. Predicted heat is based on the heat of hydration of pure phases (γ and β C_2S after [12]; C_3S triclinic after [30]), weighted for the phase proportion in each sample (see Table III).

[Tabela VII - Eventos endotérmicos de desidratação determinados por DSC. O calor previsto é baseado no calor de hidratação das fases puras (γ e β C_2S segundo [12]; C_3S triclinico segundo [30]), ponderado pela proporção em massa das fases em cada amostra (vide Tabela III).]

sample	endothermic peak at 150 °C (J/g)	endothermic peak at 425 °C (J/g)	total heat absorbed (J/g)	predicted heat absorbed (J/g)
BS 0	4.32	6.91	11.23	13.08
BS 0.5	6.05	13.91	19.96	13.98
BS 3	8.21	41.47	49.68	46.03
BS 6	13.10	67.80	80.90	70.83
BS 10	14.09	68.27	82.36	113.16

the heat of hydration of the pure phases, mentioned above.

CONCLUSIONS

Stoichiometric mixtures were prepared in order to generate C_2S (dicalcium silicate) with increasing amounts of sulfur. However, large-scale sulfur loss (from 80 to 100%) occurred probably due to large difference in the temperature of thermal decomposition of the raw materials, as calcium carbonate decomposes at much lower temperatures than calcium sulfate. This leads to early combination of calcium and silicon oxides and formation of C_2S and C_3S , and later release of SO_3 at higher temperature, in a condition that precluded a high degree of incorporation in the already crystallized calcium silicates. Quantitative phase analysis by X-ray diffraction and Rietveld method leads to reliable polymorphic recognition. Good agreement was achieved between observed and calculated diffractograms by the Rietveld method. It was demonstrated that sulfur diminishes γ C_2S abundance, increasing β C_2S accordingly. Our study

confirms that the presence of sulfur alone does not stabilize the α C_2S , the polymorph stable at highest temperature, as already mentioned [11]. The increase in C_3S abundance in samples with higher amounts of sulfur in the starting composition is not a chemical effect of sulfur, but is rather due to chemical unbalance after sulfur loss by sintering. Sulfur is known to cause shrinkage of the C_3S stability field in the $CaO-SiO_2-Al_2O_3-Fe_2O_3$ phase diagram [31]. Structural refinement of the crystalline phases by XRD-Rietveld confirm the preferential uptake of sulfur by β C_2S , the only phase that display systematic changes in its cell parameters. The two other phases obtained (γ C_2S and C_3S) did not present significant changes in their cell parameters. This study demonstrates that the presence of sulfur stabilizes β C_2S and avoids formation of γ C_2S , which is not desired in Portland clinker because of its very low reactivity with water. Thermal analysis was strongly biased by the presence of C_3S among the phases in the experiments. Notwithstanding, endothermic reactions are in agreement with the expected values of the pure phases weighted by their relative

abundance in each sample.

ACKNOWLEDGEMENTS

We are grateful to CAPES for the M.Sc. grant provided to S. D. Gomes. Prof. Paiva-Santos is acknowledged for his suggestions on Rietveld refinement strategies.

REFERENCES

- [1] J. I. Bhatti, F. M. Miller, S. H. Kosmatka, "Innovations in Portland cement manufacturing", 1st Ed., Portland Cement Association, Washington DC, USA (2004) 403.
- [2] K. Kolovos, P. Loutsi, S. Tsivilis, G. Kakali, *Cement Concrete Res.* **31** (2001) 425-429.
- [3] H. F. W. Taylor, *Cement Concrete Res.* **29** (1999) 1173-1179.
- [4] F. M. Miller, F. J. Tang, *Cement Concrete Res.* **26** (1996) 1821-1829.
- [5] D. S. Fortsch, Conference Record, Cement Industry Technical Conference, IEEE-IAS/Portland Cement Association (2004) 103-109.
- [6] A. Neville, *Cement Concrete Res.* **34** (2004) 1275-1296.
- [7] K. Morsli, A. G. de la Torre, M. Zahir, M. A. G. Aranda, *Cement Concrete Res.* **37** (2007) 639-646.
- [8] A. M. Il'inets, M. Y. A., *Sovietic Physics Crystallography (English Translation)* **35** (1990) 54-56
- [9] W. G. Mumme, R. J. Hill, G. Bushnell-Wye, E. R. Segnit, *Neues Jahrbuch für Mineralogie (Abhandlungen)* **169** (1995) 35-68.
- [10] W. G. Mumme, L. Cranswick, B. Chakoumakos, *Neues Jahrbuch für Mineralogie (Abhandlungen)* **170** (1996) 171-188.
- [11] A. Gies, D. Knöfel, *Cement Concrete Res.* **17** (1987) 317-328.
- [12] R. Müller, J. Neubauer, F. Götz-Neunhoeffler, Proc. 11th Int. Cong. Chemistry of Cement, South Africa (2003) 1043-1051.
- [13] Z. Lu, K. Tan, *Cement Concrete Res.* **27** (1997) 989-993.
- [14] A. K. Chatterjee, *Cement Concrete Res.* **26** (1996) 1213-1237.
- [15] C. D. Popescu, M. Muntean, J. H. Sharp, *Cement Concrete Composites* **25** (2003) 689-693.
- [16] D. Balzar, N. Audebrand, M. Daymond, A. Fitch, A. Hewat, J. I. Langford, A. Le Bail, D. Louër, O. Masson, C. N. McCowan, N. C. Popa, P. W. Stephens, B. Toby, *J. Appl. Crystallography* **37** (2004) 911-924.
- [17] A. C. Larson, R. B. Von Dreele, General Structure Analysis System (GSAS), Los Alamos National Laboratory Report LAUR, Los Alamos, USA (2004) 86-748.
- [18] B. H. Toby, *J. Appl. Crystallography* **34** (2001) 210-21.
- [19] N. I. Golovastikov, R. G. Matveeva, N. V. Belov, *Kristallografiya* **20** (1975) 721-729.
- [20] L. B. McCusker, R. B. Von Dreele, D. E. Cox, D. Louer, P. Scardi, *J. Appl. Crystallography* **32** (1999) 36-50.
- [21] L. A. Gobbo, L. M. Sant'Agostino, L. L. Garcez, *Cement Concrete Res.* **34** (2004) 657-664.
- [22] Y. Kihara, H. Uchikawa, *Ceramica* **32** (1986) 207-210.
- [23] G. Narsimhan, *Chem. Eng. Sci.* **16** (1961) 7-20.
- [24] A. W. D. Hills, *Chem. Eng. Sci.* **23** (1968) 297-320.
- [25] B. V. L'vov, *Thermochim. Acta* **386** (2002) 1-16.
- [26] D. L. Hudson-Lamb, C. A. Strydom, J. H. Potgieter, *Thermochim. Acta* 282/283 (1996) 483-492
- [27] V. S. Ramachandran, "Applications of differential thermal analysis in cement chemistry", 1st Ed., Chemical Publ. Co., New York, USA (1969) 308.
- [28] R. Jenkins, R. L. Snyder, "Introduction to X-ray powder diffractometry", 1st Ed., John Wiley and Sons, New York, USA (1996) 544.
- [29] R. D. Shannon, C. T. Prewitt, *Acta Crystallographica* **B52** (1968) 925-946.
- [30] J. Bensted, G. J. Audley, P. N. Aukett, *Cement Concrete Res.* **25** (1995) 426-432.
- [31] S. Uda, E. Asakura, M. Nagashima, *J. Am. Ceram. Soc.* **81** (1998) 725-729.
- (*Rec. 16/10/2009, Rev. 22/02/2010, Ac. 22/05/2010*)